RSC Advances

ROYAL SOCIETY OF CHEMISTRY

www.rsc.org/advances

Converting Obsolete Copy Paper to Porous Carbon Materials with Preeminent Adsorption Performance of Tetracycline Antibiotic

Atian Xie[a], Jiangdong Dai[a], Jinsong He[a], Jun Sun[a], Zhongshuai Chang[a], Chunxiang Li[a]* and Yongsheng Yan[a,b]*

[a] School of Chemistry and Chemical Engineering, Jiangsu University, Zhenjiang 212013, China

[b] Key Laboratory of Preparation and Applications of Environmental Friendly Materials (Ministry of Education), Jilin Normal University, Siping 136000, China

Corresponding Author: Chunxiang Li

E-mail: ujsxat@163.com

Telephone Number: +86 0511-88790683; fax: +86 0511-88791800

Abstract

Up to now, the developed adsorbents are still limited to employ for antibiotic wastewater treatment practices, due to the low adsorption capacity, slow kinetics and especially high cost. Thus, in this work, we first reported the conversion of obsolete copy paper to highly porous carbon materials (PCMs) *via* low-temperature carbonization and alkali activation two-step method. The influence of activation temperature and KOH content on the porosity and adsorption capacity of PCMs was also studied. Notably, copy paper (CP) is consumed in a extreme large quantity with a high proportion being obsoleted, which mainly consists of micro- and nano- cellulose fibers and can be used as ideal carbon source. The PCMs were characterized by several techniques and methodologies. The PCMs-850-4 exhibited an ultrahigh BET surface area of 3598.95 m^2/g and total pore volume of 1.887 cm^3/g. The influence of temperature, initial concentration, contact time, pH and ionic strength on the adsorption of PCMs-850-4 to tetracycline (TC) from water was investigated by the batch adsorption studies. The analysis of adsorption isotherm, kinetics and thermodynamics property was conducted to understand the adsorption behavior. The equilibrium experimental data was fitted to Langmuir model well and the kinetic data was best described by the pseudo-second-order rate model. Importantly, the PCMs-850-4 displayed an ultrahigh adsorption amount of 1437.76 mg/g at 298 K, and increasing temperature was benefited for adsorption. Also, fast kinetics and great regeneration made the PCMs-850-4 as promising adsorbents for the low-cost, highly efficient and fast removal of organic pollutants from water environments.

Keywords: Obsolete Copy Paper, Alkali Activation, Porous Carbon Materials, Adsorption, Tetracycline Antibiotic, Biomass Materials

1. Introduction

Antibiotics discharged into the environment have brought increasing attentions because they have been proved to be a class of potent pollutants.[1] Most of antibiotics cannot be completely metabolized and absorbed by organisms and a large proportion excreted through urine and feces still maintain biological activity.[2] Tetracycline (TC) is utilized extensively for human therapy and farming industry and also used as food additive to protect disease, as shown in Fig. 1, which contains tricarbonylamide, phenolic diketone and dimethylamine groups.[3] The widespread use of TC has became a rigorous issue and posed a variety of undesirable effects, such as cancer, acute and chronic toxicity, and antibiotic resistance of microorganisms. Residues of TC were frequently detected in soil, surface water, groundwater, and even drinking water.[4, 5] There are many treatment methods of pharmaceutical antibiotics removal from wastewaters, such as chemical precipitation,[6] degradation,[7] bioremoval,[8] adsorption,[9] chemical oxidation/reduction,[10] and membrane filtration.[11] Adsorption has the advantages of easy handling, high efficiency and economic feasibility, etc. The excellent property and high efficiency of adsorbents is important for the removal of TC. Activated carbons are usually utilized as adsorbent to remove contaminations from wastewater, *via* the π-π conjugation, van der Waals force, electrostatic interaction, or chemical bonds.[12, 13] However, large scale application of commercial activated carbon is hindered due to their high cost and poor reusability. Hence, the development of economic, eco-friendly and more efficient adsorbents to remove TC is an urgent research subject.[14-16]

Porous carbon materials (PCMs) are considered as promising materials for applications in many fields, especially as special adsorbents for wastewater purification,[17] owing to their large specific surface area, high physicochemical stability, high adsorption capacity, high mechanical strength and high degree of surface reactivity.[18] Mass consumption of fossil fuels and increasing growth of environmental problems have brought people's great attentions, which have realized the importance of exploiting sustainable production of fuels, chemicals and materials,[19-21] and strove to minimize contaminations such as toxic gases emissions[22] and solid wastes processing[23, 24]. With the advent era of information, copying has gradually replaced artificial handwritten so that the amount of copy paper (CP) is on the rise and enormous. Nevertheless, how to deal with the waste CP has become a serious problem. The principal component of CP is plant fiber, including

cellulose, hemicelluloses and lignin, which are ideal carbon precursor for preparation of PCMs as adsorbents to remove pollutants. In a deep sense, renewable cellulose, hemicelluloses, and lignin are the most abundant biomass materials with excellent properties, such as easy availability, biodegradable and non-pollution. The microstructure of CP is composed of a large number of belts and filamentous fibers in micro- and nano size, which are benefited for alkali activation process to produce a large number of micropores. Therefore, CP is a more ideal precursor for preparation of PCMs.

Currently, there is no doubt that biomass is the cost-optimal precursor for the preparation of PCMs. For example, Alessandro C. Martins et al. reported that NaOH-activated carbon produced from macadamia nut shells showed the maximum monolayer adsorption capacity (Q_m) of 455.33 mg/g for TC.[25] Thawatchai Maneerung et al. reported activated carbon derived from carbon residue from biomass gasification to remove Rhodamine B, with the maximum monolayer adsorption capability of 189.83 mg/g.[26] Sandro Altenor et al. prepared activated carbon using vetiver roots as precursor by chemical activation for adsorption of methylene blue and phenol.[27] However, to the best of our knowledge, literatures about the use of obsolete CP as carbon precursor to prepare PCMs have not been reported.

Herein, we fabricated high-performance PCMs using obsolete CP as renewable biomass processor, which were expected to display fast kinetics, good regeneration capacity and excellent environmental adaptability on TC removal, with a huge potential possibility for large-scale application in wastewater treatment. More importantly, this work provided new insight into the preparation of advanced adsorbents and the utilization of biomass resources, which was of great significance for environment and energy fields. Additionally, the PCMs were promising materials not only for wastewater treatment, but also for energy storage and conversion, and catalysis applications.

2. Experimental

2.1. Materials and Chemicals

Tetracycline hydrochloride (TC, 98 %) was obtained from Aladdin Industrial Corporation (Shanghai, China), and stored in dark at 2-8 °C. Waste copy papers were obtained from daily office. KOH (AR, 96 %), KBr (AR, 99 %) and HCl (36–38 %) were obtained from Sinopharm

Chemical Reagent Co., Ltd. (Shanghai, China). All chemicals were of analytical reagent grade and used directly without any further purification. The water used in all experiments was deionized water.

2.2. Instruments and Characterization Methods

The carbonization and activation was carried out in a tube furnace (SK-GO6123K, Tianjin, China). Samples elemental analysis was offered by an element analyzer (FLASH1112A, CE, Italy). The microtexture and morphology were analyzed by transmission electron microscopy (TEM; IEM-200CX, JEOL, Japan) and scanning electron microscope (SEM; JSM-7001F, JEOL, Japan). Fourier transform infrared spectra were recorded on a Tensor FTIR spectrometer (FT-IR; Nicolet Nexus 470, USA). X-ray diffraction (XRD) analysis was taken on a X-ray diffractometer (Bruker D8 Advance, Bruker AXS, Germany) using Cu Kα radiation (λ = 1.5406 Å, 40 KV, 40 mA) and the data were collected from 2θ = 10-70° at a scan rate of 7° min^{-1} for phase identification. Raman spectra were analyzed using a Laser Raman Spectrometer (DXR, Thermo Fisher, USA) with a 532 nm wavelength incident laser light and 10 mW power. The N_2 adsorption-desorption isotherms measure was using a BELSORP instrument (BEL, Japan, Inc.) at 77 K. X-ray photoelectron spectroscopy (XPS) analysis was conducted in a Kratos Axis Ultra DLD spectrometer with the excitation of X-ray provided by a monochromatic source of Al Kα (1486.6 eV).

2.3. Preparation of PCMs

In brief, the CP was carbonated in a tube furnace at the ramp of 5 °C/min from RT to 500 °C and maintained at 500 °C for 2 h in nitrogen atmosphere. The carbonized CP (CCP) was obtained and stored for further use. Subsequently, the CCP was sufficiently ground with activation agent KOH at a mass ratios of 1:4 (CCP:KOH) and the obtained mixture were thermal treatment at desirable temperatures varying from 750 to 900 °C for 1 h in a tube furnace under the protection of nitrogen, with a heating ramp of 5 °C/min. Finally, the resultants were soaked in 2 M HCl to eliminate impurity. The PCMs were collected *via* vacuum filtration, washed several times with deionized water to neutral, and then dried in oven at 80 °C for 12 h. The influence of KOH content for PCMs was also studied. The preparation method was same as above-mentioned, excepting that the mass ratios of CCP and KOH was varied from 1:1 to 1:5 at 850 °C. (Labeled as PCMs-T-x, T and x represent temperature and mass ratios, respectively.)

2.4. Bath adsorption Experiments

All batch experiments were carried out using 10 mL of centrifuge tube containing 2 mg of PCMs-850-4 and 10 ml of TC solutions in the dark and all of the tests were carried out in triplicate. Supernatant were obtained through a 0.45 μm membrane filter and determined by an UV–Vis spectrophotometer (Agilent Cary 8454 UV-Vis) at a fixed wavelength of 357 nm. Our preliminary study (adsorbent free) indicated that the loss of TC owing to filter interception was far less than 4 % under the applied experiment condition (data not shown).

The adsorption isotherms were performed using TC solutions with the initial concentrations ranging from 50 to 350 mg/L at 298, 308 and 318 K for 12 h to reach equilibrium, respectively. The equilibrium absorption amount Q_e (mg/g) was calculated by the following equation:

$$Q_e = \frac{(C_0 - C_e)V}{M} \qquad (1)$$

The kinetic studies were investigated at appropriate time intervals of 1 to 90 min using 100, 150 and 200 mg/L TC solutions at 298 K, respectively. The absorption amount at t time Q_t (mg/g) was calculated by the following equation:

$$Q_t = \frac{(C_0 - C_t)V}{M} \qquad (2)$$

Herein, C_0 and C_t (mg/L) are beginning and at any time concentrations of TC, respectively. C_e (mg/L) is concentrations of TC at equilibrium conditions. V (L) is volume of the TC solution and M (g) is mass of the PCMs-850-4.

To further study the adsorption of TC onto PCMs-850-4, we investigated the effect of solution pH value and ionic strength on adsorption. The experiments were conducted using 250 mg/L TC solution. The solution pH values were in a range from 2 to 6, which were adjusted by 0.1 mol/L NaOH and 0.1 mol/L HCl solutions. Moreover, different concentrations of NaCl contents were 0.05, 0.2, 0.4, 0.6, 0.8 and 1.0 M, respectively. The above solutions were used for adsorption at 298 K for 12 h to reach equilibrium.

3. Results and Discussion

Fig. 2 shows the influence of activation temperature and KOH content on porosity and adsorption capacity of PCMs and different parameters of porosity characteristics are listed in

Table 1. The result of Fig. 2a indicated activation temperature significant influenced the porosity of PCMs. BET surface area increased with the increase of temperature from 2978.44 m^2/g to 3598.95 m^2/g, but decreased to 3344.58 m^2/g when the temperature reached 900 °C. The reaction of carbon and KOH might overreact at high temperature and resulted in the increase of pore size and decrease of BET surface area, naturally, leading to decline the adsorption capacity for TC. As shown in Fig. 2a, we could find the PCMs-900-4 had a large number of mesoporous. From the inset of Fig. 2a, the pore size increased with the increasing temperature, which confirmed the above-mentioned speculation. Meanwhile, BET surface area increased with the increase of KOH content (N_2 adsorption-desorption isotherm of PCMs-850-5 was not provided because of ultra-low yield of about 2 %). The pore size also showed a trend of rise with the increase of the KOH content (from inset of Fig. 2b). Above results showed the activation temperature and KOH content had a significant influence on porosity of PCMs. Fig. 2c-d indicated the PCMs-850-4 displayed the optimal adsorption capacity. Combining all above results, we could find the porosity of PCMs was crucial for adsorption performance of TC. Therefore, the PCMs-850-4 was chosen for further investigation in the following adsorption experiments.

We conducted scanning electron microscopy (SEM) test for the synthesized PCMs-850-4. SEM images of CP, CCP and PCMs-850-4 are shown in Fig. 3. It was observed that the CP was made up of many stacked ribbons with some impurity and possessed relatively smooth surface. From Fig. 3b, it is clear that the stack was not sealed, ribbons mutual crisscross with abundant space. Fig. 3c, d revealed the CCP still maintained original morphology but surface became roughness with wrinkle and lamellar structures. The structure of PCMs-850-4 was undergone tremendous changes. The ribbons become fragment in the activation process. Moreover, the surface of bulks changed harsher and the layer structure was more obvious. The results implied that PCMs-850-4 possessed abundant porous structure. The morphology of PCMs-850-4 was further investigated by TEM. PCMs-850-4 (in Fig. 4a) had the presence of a large number of pores, and meanwhile belt-like and some layered structure also could be observed in Fig. 4b, which were matched well with the results of SEM images.

In order to further analyze the porosity of PCMs-850-4, the N_2 sorption isothermal measure was conducted. Strong N_2 adsorption of PCMs-850-4 exhibited a combined type-I/IV adsorption

isotherms (Fig. 5a). This behavior was widely different from the I-type of traditional activated carbon according to N_2 adsorption-desorption isotherms,[28] which was representative combination of microporous and mesoporous. We could observe a blurry capillary condensation phenomenon in a relative pressure range of 0.15-0.30, which was typically mesoporous. The specific surface area of PCMs-850-4 calculated by the BET method was 3598.95 m^2/g with the micro porosity of 91.77%, which could provide a large amount of active site for TC molecular. The inset of Fig. 5a exhibited the pore size distributions, which were analyzed by DFT method. The pore size had a concentrated distribution range of 1.766-2.313 nm and the micropores were concentrated at 1.76 nm. The total pore volume of PCMs-850-4 was calculated to be 1.887 cm^3/g and the mean pore diameter was 2.002 nm. The large volume of the PCMs-850-4 was significantly favorable for rapid diffusion of TC molecular, resulting in an exceptionally fast rate for adsorption process. Furthermore, the high proportion of micropores was extremely beneficial for micropore filling.[29] However, as shown in Fig. 5b, the BET surface area (<25 m^2/g) of CP and CCP was negligible relative to PCMs-850-4. Correspondingly, the adsorption capacity (<30 mg/g) of CP and CCP for TC was very little (as shown in Fig. S1). The results indicated KOH was crucial for porosity and adsorption capacity of PCMs-850-4.

The phase structure of CCP and PCMs-850-4 was characterized by XRD and Raman spectroscopy. Fig. 6a shows the XRD diffraction patterns of CCP and PCMs-850-4. The XRD patterns revealed the CCP and PCMs-850-4 with very low crystalline order. We could find two wide diffraction peaks in the patterns of PCMs-850-4. One of them was located at 22–26° and corresponded to the (002) crystal plane.[30, 31] The other feature band with weak intensity contributed to the combined action of diffraction peaks (100) and (101) crystal plane. Abundant pore structures (primarily micropores) continuously scattered the X-ray radiation and led to the increasing background in the 2θ range between 10 and 39°,[32] which was consistent with textural data of the produced porosity in the activation process. However, the patterns of CCP had only one wide diffraction peaks located at 22–26° and corresponds to the (002) crystal plane, indicating only existence of amorphous carbon structure. The results demonstrated that PCMs-850-4 had most amorphous carbon structure and a certain trend of graphitization.

The Raman spectra of CCP and PCMs-850-4 are shown in Fig. 6b. Two prominent broad

bands were located around at 1580 (G band) and 1350 cm^{-1} (D band), which were corresponding to graphitic lattice vibration mode and disorder in the graphitic structure, respectively. We could conveniently estimate the degree of graphitization by the intensity ratio of *G*/*D* peak (I_G/I_D).[33] The higher I_G/I_D ratio values, the higher degree of ordering. The I_G/I_D ratios were 0.69 for CCP and 0.97 for PCMs-850-4, revealing the CCP treatment with KOH results in increasing disorder, which was caused by potassium vapor intercalation into carbon layer in activation process. The activation reaction was listed as following:[34]

$$6KOH + 2C=2K + 3H_2 + 2K_2CO_3$$

XPS test was conducted to probe the chemical identification of the elements in the CCP and PCMs-850-4. The results agreed well with the elemental analysis (Table S1). It can be seen that there was C 1s and O 1s peaks from the survey scan spectra (Fig. S2). The spectra for C1s spectrum (Fig. 7a,c) with three peaks at 284.5, 284.83 and 286.8 eV, which were attributed to C–C, C=C, C–O and C=O,[35, 36] respectively. The three peaks fitted well to O 1s spectra (Fig. 7b,d) of two samples were located at 531.3, 532.4 and 533.7 eV, which were corresponding to C=O, H–O and C–O–C,[37-39] respectively. It's noteworthy that the present forms of carbon had no evident change while obvious changes were taken place in the oxygen after carbonization (in Table S2). These results strongly proved that the PCMs-850-4 possessed rich oxygen-containing groups, benefiting for the interactions with TC molecules.

FT-IR spectra of CCP and PCMs-850-4 are shown in Fig. S3. As can be seen in the spectrum of CCP, the broad absorbance between 500 and 1650 cm^{-1} was attributed to the C–C, C=C, C–O and O–H bending vibrations, respectively.[40] We also could observe an extremely weak peak at 1780 cm^{-1} (C=O). The weak absorbance peak at 2930 cm^{-1} was ascribed to $–CH_2–$ stretching vibrations. Obviously, the band at 3440 cm^{-1} was from the O−H stretching vibrations. However, the spectrum of PCMs-850-4 did not have obvious change, and the peak intensity of O−H bound slightly decreased, indicating the decrease of hydrogen and oxygen element. These results agreed well with the XPS analysis and elemental analysis.

Adsorption of TC

Adsorption isotherm describes that how adsorbate molecules are distributed between the solid and liquid phases when the adsorption system reach equilibrium state.[41] Langmuir isotherm

model hypothesize that adsorbate onto adsorbents surface is monolayer adsorption, while Freundlich isotherm model different from Langmuir isotherm is multilayer adsorption.[42, 43] Basically, adsorption isotherms indicate that how interact between adsorbate and adsorbents, being important for optimizing the use of adsorbents.

Adsorption Isotherm. Langmuir model was employed to analyze the adsorption data of TC onto the PCMs-850-4, the linear equation was described as follow:

$$\frac{C_e}{Q_e} = \frac{1}{K_L Q_m} + \frac{C_e}{Q_m} \quad (3)$$

Herein, Q_m (mg/g) is the maximum adsorption capacity of Langmuir monolayer adsorption. K_L (L/mg) is the Langmuir constant. The parameters of Langmuir together with coefficients are recorded in Table 2. Obviously, the data obtained from experiment was well fitted with Langmuir model ($R^2 > 0.99$), indicating the adsorption process of TC onto PCMs-850-4 occurs upon a homogeneous surface where the TC was distributed monolayer. The linear and non-linear fitting of Langmuir at different temperatures are displayed in Fig. 8. Langmuir model could be better fitted to data of adsorption isotherms *via* linear fitting (Fig. 8b). Non-linear fitting suggested that Langmuir fitting values were more consistent with the experimental values. Furthermore, the adsorption capacity ($Q_{e,exp}$) of TC onto PCMs-850-4 in aqueous solutions were 1437.76 mg/g at 298K. Here, the obtained carbon in this work showed a higher adsorption amount of TC than other reported adsorbents.[25, 44-48] (listed in Table 5)

In order to estimate the thermodynamic parameters, TC adsorption performance onto PCMs-850-4 experiments were performed at different temperatures. From Fig. 8a, we could easily find that the adsorption capacity increased from 1437.76 to 1644.82 mg/g with temperature elevated from 298 to 318 K. The change of Gibbs free energy (ΔG^θ), standard enthalpy (ΔH^θ) and entropy (ΔS^θ) were calculated using the following formulas:

$$\Delta G^\theta = -RT\ln(K_0) \quad (4)$$

$$\Delta G^\theta = \Delta H^\theta - T\Delta S^\theta \quad (5)$$

K_0 is defined as follows:

$$K_0 = \frac{a_s}{a_e} = \frac{v_s}{v_e}\frac{Q_e}{C_e} \quad (6)$$

Where R (8.314 J/mol·K) is the universal gas constant and T (K) is the temperature of the solution. a_s is the activity of adsorbed TC and a_e is the activity of TC in solution at equilibrium. Q_e (mg/g) is the amount of TC adsorbed by per unit mass of PCMs-850-4, v_s is the activity coefficient of the adsorbed TC and v_e is the activity coefficient of TC in solution. With decreasing TC concentration to zero gradually in the solution, thus, as shown in Fig. 9a, K_0 obtained by fitting ln (Q_e/C_e) vs Q_e from the straight line intercept with the vertical axis. ΔG^θ was plotted against T to calculate ΔH^θ and ΔS^θ from the slope and intercept,[49] and the results are shown in Fig. 9b. The values of K_0, ΔH^θ, ΔS^θ and ΔG^θ at different temperatures are given in Table 3. The positive value obtained for standard enthalpy change of 1.631 kJ/mol indicated the adsorption process was endothermic, which was consistent with the results of batch experiments at different temperatures. The positive standard entropy change indicated increased randomness at the solid−liquid interface during the adsorption and the negative value of Gibbs free energy confirmed that the adsorption of TC onto PCMs-850-4 was spontaneous at the studied temperatures.[50]

Adsorption kinetics. The adsorption kinetics at the different concentrations was illustrated in Fig. 10a-c. Adsorption rapidly increased within 5 min, subsequently the adsorption rate declined and reached an equilibrium within 90 min. The adsorption rate was an important parameter to understand the adsorption dynamics. To investigate the adsorption kinetics of TC onto PCMs-850-4, pseudo-first-order and pseudo-second-order kinetic models were used to fit the experimental data.[51]

The linear expression of pseudo-first-order kinetic model was given as:

$$\ln(Q_e - Q_t) = \ln Q_e - K_1 t \qquad (7)$$

Where K_1 (min^{-1}) is the rate constant of the pseudo-first-order equation. Relevant data of adsorption kinetics are shown in Fig 10d-e and kinetic parameters are recorded in Table 4. Obviously, linearity of the pseudo-first-order mechanism is acceptable but not ideal due to the defective correlation coefficient ($R^2 < 0.999$). Thus, the pseudo-first-order kinetics was not enough to explain the rate processes.

The experimental data were further interpreted by pseudo-second-order kinetics model. The linear form could be expressed as follow:

$$\frac{t}{Q_t} = \frac{1}{K_2 Q_e^2} + \frac{t}{Q_e} \quad (8)$$

Here K_2 (g mg^{-1} min^{-1}) is the rate constant of the pseudo-second-order. The parameters are presented in Table 4. From Fig. 10e, the pseudo-second-order model could describe adsorption behavior over the whole range of adsorption ($R^2 > 0.999$), inferring that the adsorption rate of TC onto PCMs-850-4 was mainly controlled by the chemisorption.[52]

The kinetic results were further analyzed using the intra-particle diffusion model to study the adsorption process.[53] The intra-particle diffusion model equation was writing as:

$$Q_t = K_i^{1/2} + C \quad (9)$$

Where K_i [mg/(g·min$^{1/2}$)] and C are the intra-particle diffusion coefficient and intercept for the intra-particle diffusion model, respectively. The plots of analysis result obtained for Q_t versus $t^{1/2}$ are shown in Fig. S4 and the values of K_i, C_i, and R^2 at different concentrations of TC are listed in Table S3. According to intra-particle diffusion model, if the plot of Q_t versus $t^{1/2}$ is a straight line of through origin, indicating the rate limiting step is intra-particle diffusion alone. However, if the plots display multilinear, demonstrating two or more rate limiting steps involved in the sorption process. As shown in Fig. S4, the plots displayed three straight lines, which fitted well to the intra-particle diffusion model ($R^2 > 0.91$). The first straight portion expressed the diffusion of TC from the bulk solution to the solid PCMs-850-4; the second linear portion meant the intra-particle diffusion of TC into the mesopores and macropores of PCMs-850-4; the third linear portion with smaller K_i value represented the rate of adsorption adagissimo, indicating equilibrium adsorption achieved. Piecewise-linear pattern findings indicated that the adsorption of TC onto PCMs-850-4 involved in the complex mechanisms.

Effect of pH

Adsorption of TC onto the PCMs-850-4 was investigated by conducting the experiments with solution pH value ranging from 2 to 6 (Fig. 11a). It was found that the highest adsorption capacity at pH=3, and decreased from pH 3-6. The solution pH is an important impact parameter to the adsorption process owing to the change of structure of the TC molecules and the surface charge of the adsorbent.[54] According to the fractions of TC (Fig. 11b), when the pH of solution unreached the pK_{a1} (3.30) value of TC, the main specie was TC^+, but the dominant species were TC^0 when

solution pH between pK_{a1} to pK_{a2} (3.30-7.70), while the surface of PCMs-850-4 was rich in oxygen containing functional groups, which mainly existed in the negative charged form. As a rule, with the increasing pH, the TC^+ decreased and the adsorption capacity of PCMs-850-4 should be decreased. From Fig. 11a, we could find the highest adsorption capacity at pH=3, the adsorption capacity did not decrease significantly and still kept a considerable amount, implying electrostatic interaction was not only involved in adsorption process.

Effect of Ionic Strength

Ionic strength is also an impact parameter for adsorption capacity. Herein, different amounts of NaCl were added to the TC solutions to study the effect of ionic strength on the adsorption capacity.[55] As depicted in Fig. 12a, increasing NaCl concentration from 0.05 to 1.0 M led to the decrease of adsorption capacity. Competitive effect between the Na^+, Cl^- and the TC^+ with functional surface of the PCMs-850-4 might be explained this result. The shielding effects of ions for TC^+ molecules were enhanced in the higher NaCl concentration, resulting in the decrease of adsorption amount. Thus, adsorption process partially involved electrostatic interaction.

Reusability of PCMs-850-4

The regeneration of adsorbents is crucial to assess the feasibility of practical and large-scale application. The regeneration test of the PCMs-850-4 was carried out by immersing the adsorbed saturation PCMs-850-4 into NaOH (0.2M) solution for 12 h at 318 K in a constant temperature vibrator. The adsorption-desorption test was conducted continually five times, and the results are depicted in Fig. 12b. The regenerated PCMs-850-4 displayed good reusability and adsorption capacities decreased slightly, which still maintained the high adsorption capacity of 901.69 mg/g after five cycles. The PCMs-850-4 had excellent reusability for the removal of TC. The potential of the PCMs-850-4 in large-scale application for antibiotics removal will further study in our following study.

Proposed Mechanism

In general, adsorption mechanism was affected by many factors, including physicochemical properties of PCMs-850-4 (e.g. surface functional groups and pore size) and the mass-transfer process in solution. The graphite surface of PCMs-850-4 possessed a strong van der Waals force[56], which was demonstrated by the results of XRD and Raman spectroscopy. The strong van der

Waals force could happen easily between the TC and the graphite surface of PCMs-850-4. Because TC is a planar ring molecule, hence, TC could be easily adsorbed onto PCMs-850-4 *via* the π-π stacking interaction between the aromatic structure of TC and the skeleton of PCMs-850-4. However, except van der Waals force and π-π stacking interactions could contribute to the adsorption. It has been proved that the main species is TC^+ and TC^0 in acidic TC solution, thus, TC^+ could be easily adsorbed onto positively charged surface of PCMs-850-4, suggesting that electrostatic attraction partially contributed to TC adsorption onto PCMs-850-4. More importantly, there are many functional groups in surface of PCMs-850-4, such as –OH, C=O, which was demonstrated by the results of FT-IR and XPS spectroscopy, therefore, hydrogen binding and chemical reaction may occur. Remarkably, ultrahigh BET surface area provided a large number of sites for above-mentioned interaction of TC adsorbed onto PCMs-850-4. In conclusion, TC adsorption onto PCMs-850-4 was a complicated process, involving the physical and chemical processes. More detailed adsorption mechanisms need further in-depth study.

4. Conclusions

In summary, we reported the synthesis of PCMs *via* a two-step method, namely carbonized and alkali activated process. Owing to their large surface area, highly porous structure, and rich oxygen containing functional groups, the as-prepared PCMs-850-4 exhibited high adsorption capacity (Q_m) of 1437.76 mg/g at 298K. Batch adsorption experiments indicated that the PCMs-850-4 were effective and rapid in removing TC. Moreover, the PCMs-850-4 displayed excellent reusability after extended regeneration cycles, demonstrating that the adsorbent could be long-term and large scale application in practical. Considering the facile synthetic process and accessible raw materials, and the high adsorption capacity, ultrafast adsorption rate, and good reusability, the PCMs have great promise as the highly efficient and environmental friendly adsorbent in the removal of antibiotics and other organic contaminants.

Acknowledgments

This work was financially supported by the National Natural Science Foundation of China (Nos. 21277063 and 21407058, 21446015, 21546013, U1510126), the National Basic Research Program of China (973 Program, 2012CB821500), Natural Science Foundation of Jiangsu Province (BK20140534), Research Fund for the Doctoral Program of Higher Education of China

(20133227110022 and 20133227110010) and Jiangsu Planned Projects for Postdoctoral Research Funds (1102119C).

REFERENCES

1 M. B. Ahmed, J. L. Zhou, H. H. Ngo and W. Guo, *Sci.Total Environ.*, 2015, **532**, 112–126.
2 X. D. Zhu, Y. J. Wang, R. J. Sun and D. M. Zhou, *Chemosphere*, 2013, **92**, 925-932.
3 Z. Zhang, H. Lan, H. Liu, H. Li and J. Qu, *RSC Adv.*, 2015, **5**, 42407-42413.
4 L. Ji, W. Chen, L. Duan and D. Zhu, *Environ. Sci. technol.*, 2009, **43**, 2322-2327.
5 Y. J. Wang, D. A. Jia, R. J. Sun, B. J. Zhu and D. M. Zhou, *Environ. Sci. Technol.*, 2008, **42**, 3254-3259.
6 C. Li, Z. Zhuang, H. Feng, Z. Wu, Y. Hong and L. Zhang, *ACS Appl. Mater. Interf.*, 2013, **5**, 9719-9725.
7 Z. Zhang, J. Hao, W. Yang, B. Lu, X. Ke, B. Zhang and J. Tang, *ACS Appl. Mater. Interf.*, 2013, **5**, 3809-3815.
8 T. t. Burcu Ertit, K. Sevgi Ertu?rul and D. n. G?nül, *Water Sci. Technol.*, 2012, **66**, 2177-2184.
9 J. Dai, J. Pan, L. Xu, X. Li, Z. Zhou, R. Zhang and Y. Yan, *J. Hazard. Mater.*, 2012, 205-206, 179–188.
10 B. Li, Y. Dong, C. Zou and Y. Xu, *Ind. Eng. Chem. Res.*, 2014, **53**, 4199-4206.
11 X. Wei, K. Xin, S. Wang, X. Hai, J. Wang and J. Chen, *Ind. Eng. Chem. Res*, 2013, **52**, 17583-17590.
12 D. J. D. Ridder, L. Villacorte, A. R. D. Verliefde, J. Q. J. C. Verberk, S. G. J. Heijman, G. L. Amy and J. C. V. Dijk, *Water Res.*, 2010, **44**, 3077–3086.
13 G. K. Ramesha, A. V. Kumara, H. B. Muralidhara and S. Sampath, *J. Colloid Interf. Sci.*, 2011, **361**, 270-277.
14 G. Magnacca, A. Allera, E. Montoneri, L. Celi, D. E. Benito, L. G. Gagliardi, M. C. Gonzalez, D. O. Mártire and L. Carlos, *ACS Sustain. Chem. Eng.*, 2014, **2**, 1518-1524.
15 S. Nayab, A. Farrukh, Z. Oluz, E. Tuncel, S. R. Tariq, R. H. Ur, K. Kirchhoff, H. Duran and B. Yameen, *ACS Appl. Mater. Interf.*, 2014, **6**, 4408-4417.
16 Y. Kuwahara, S. Tamagawa, T. Fujitani and H. Yamashita, *J. Mater. Chem. A*, 2013, **1**, 7199-7210.
17 B. Wang, W. Chen, H. Fu, X. Qu, S. Zheng, Z. Xu and D. Zhu, *Carbon*, 2014, **79**, 203-212.
18 M. A. Yahya, Z. Al-Qodah and C. W. Z. Ngah, *Renew. Sust. Energ. Rev.*, 2015, **46**, 218-235.
19 Y. Q. Li, Y. A. Samad, K. Polychronopoulou, S. M. Alhassan and K. Liao, *ACS Sustain. Chem. Eng.*, 2014, **2**, 1492-1497.
20 C. Wu, L. Wang, P. T. Williams, J. Shi and J. Huang, *Appl. Catal. B-Environ.*, 2011, **108**, 6-13.
21 M. M. Titirici, R. J. White, C. Falco and M. Sevilla, *Energ. Environ. Sci.*, 2012, **5**, 6796-6822.
22 R. Zhou, G. Hu, R. Yu, C. Pan and Z. L. Wang, *Nano Energy*, 2015, 588–596.
23 S. Hu and Y. L. Hsieh, *Acs Sustainable Chem Eng*, 2014, **2**, 726-734.
24 T. A. Hassan, V. K. Rangari and S. Jeelani, *ACS Sustain. Chem. Eng.*, 2014, **2**, 706-717.
25 A. C. Martins, O. Pezoti, A. L. Cazetta, K. C. Bedin, D. A. S. Yamazaki, G. F. G. Bandoch, T. Asefa, J. V. Visentainer and V. C. Almeida, *Chem. Eng. J.*, 2015, **260**, 291-299.
26 T. Maneerung, J. Liew, Y. Dai, S. Kawi, C. Chong and C.-H. Wang, *Bioresource Technol.*, 2016, **200**, 350-359.
27 S. Altenor, B. Carene, E. Emmanuel, J. Lambert, J. J. Ehrhardt and S. Gaspard, *J. Hazard.*

Mater., 2009, **165**, 1029-1039.
28 Y. Young Soo, C. Se Youn, S. Jinyong, K. Byung Hoon, C. Sung-Jin, B. Seung Jae, H. Y. Suk, T. Yongsug, P. Yung Woo and P. Sungjin, *Adv. Mater.*, 2013, **25**, 1993-1998.
29 Y. Zhang, X. Ma and R. Yong, *Environ. Pollut.*, 2014, **185**, 213-218.
30 R. H. Bragg and M. L. Hammond, *Carbon*, 1965, **3**, 340.
31 B. E. Warren and P. Bodenstein, *Acta Crystallogr.*, 1965, **18**, 282-286.
32 R. Diduszko, A. Swiatkowski and B. J. Trznadel, *Carbon*, 2000, **38**, 1153–1162.
33 A. C. Ferrari, *Phys. Rev. B*, 2000, **61**, 14095-14107.
34 E. Raymundo-Piñero, P. Azaïs, T. Cacciaguerra, D. Cazorla-Amorós, A. Linares-Solano and F. Béguin, *Carbon*, 2005, **43**, 786-795.
35 C. Hinnen, D. Imbert, J. M. Siffre and P. Marcus, *Appl. Surf. Sci.*, 1994, **78**, 219-231.
36 T. R. Gengenbach, R. C. C. And and H. J. Griesser, *Surf. Interface Anal.*, 1996, **24**, 271–281.
37 L. T. Weng, C. Poleunis, P. Bertrand, V. Carlier, M. Sclavons, P. Franquinet and R. Legras, *J. Adhes. Sci. Technol.*, 1995, **9**, 859-871.
38 M. J. Goldberg, J. G. Clabes and C. A. Kovac, *J. Vac. Sci. Technol. A*, 1988, **6**, 991 - 996.
39 C. Jones and E. Sammann, *Carbon*, 1990, **28**, 509–514.
40 C. Zaiming, C. Baoliang and C. T. Chiou, *Environ. Sci. Technol.*, 2012, **46**, 11104-11111.
41 I. A. W. Tan, A. L. Ahmad and B. H. Hameed, *J. Hazard. Mater.*, 2008, **154**, 337-346.
42 I. Langmuir, *J. Am. Chem .Soc*, 1918, **40**, 1361-1403.
43 H. M. F. Freundlich, *J. Phys. Chem.*, 1906, **57**, 385−471.
44 K. Pankaj, R. F. Giese and D. S. Aga, *Environ. Sci. Technol.*, 2004, **38**, págs. 4097-4105.
45 Z. Li, P. H. Chang, J. S. Jean, W. T. Jiang and C. J. Wang, *J. Colloid Interf. Sci.*, 2010, **341**, 311-319.
46 J. Rivera Utrilla, C. V. Gómez Pacheco, M. Sánchez Polo and R. Ocampo Pérez, *J. Environ. Manag.*, 2013, **131**, 16–24.
47 G. Li, D. Zhang, M. Wang, J. Huang and L. Huang, *Ecotoxi. Environ. safe.*, 2013, **98**, 273-282.
48 Y. Gao, Y. Li, L. Zhang, H. Huang, J. Hu, S. M. Shah and X. Su, *J. Colloid Interf. Sci.*, 2012, **368**, 540-546.
49 J. Shah, M. R. Jan, A. U. Haq and M. Zeeshan, *J. Saudi Chem. Soc.*, 2012.
50 H. T. Fan, X. Fan, J. Li, M. Guo, D. Zhang, F. Yan and T. Sun, *Ind. Eng. Chem. Res.*, 2012, **51**, 5216-5223.
51 Y. S. Ho, J. C. Y. N. Mckay and G., *Sep. Purif. Rev.*, 2011, **29**, 189-232.
52 Y. Ge, X. Cui, D. Xiao and Z. Li, *J. Mater. Chem.*, 2014, **2**, 2136-2145.
53 W. J. Weber and J. C. Morris, *J. Sanit. Eng. Div.*, 1963, **89**, 31-60.
54 G. Cheng and K. G. Karthikeyan, *Environ. Sci. Technol.*, 2005, **39**, 2660-2667.
55 J. Ma, F. Yu, L. Zhou, L. Jin, M. Yang, J. Luan, Y. Tang, H. Fan, Z. Yuan and J. Chen, *ACS Appl. Mater. Interf.*, 2012, **4**, 5749-5760.
56 L. Ji, W. Chen, L. Duan and D. Zhu, *Environ. Sci. Technol.*, 2009, **43**, 2322-2327.

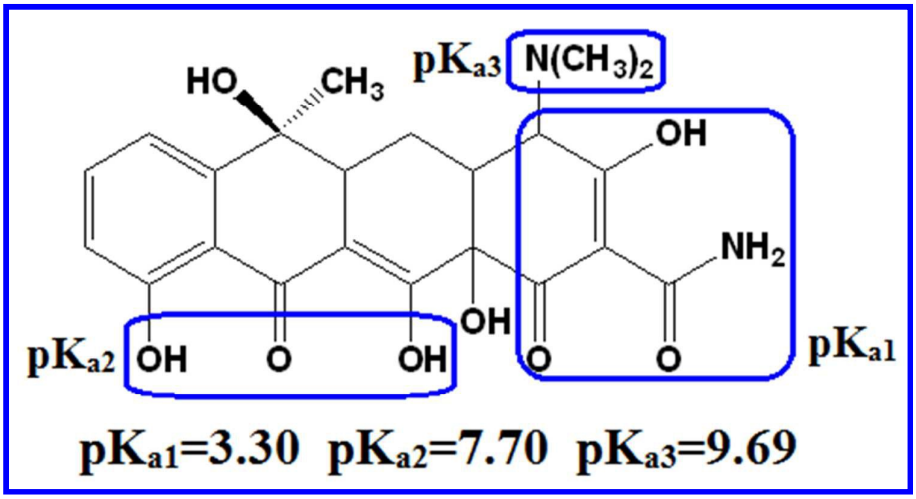

Fig. 1 The molecular structure of TC.

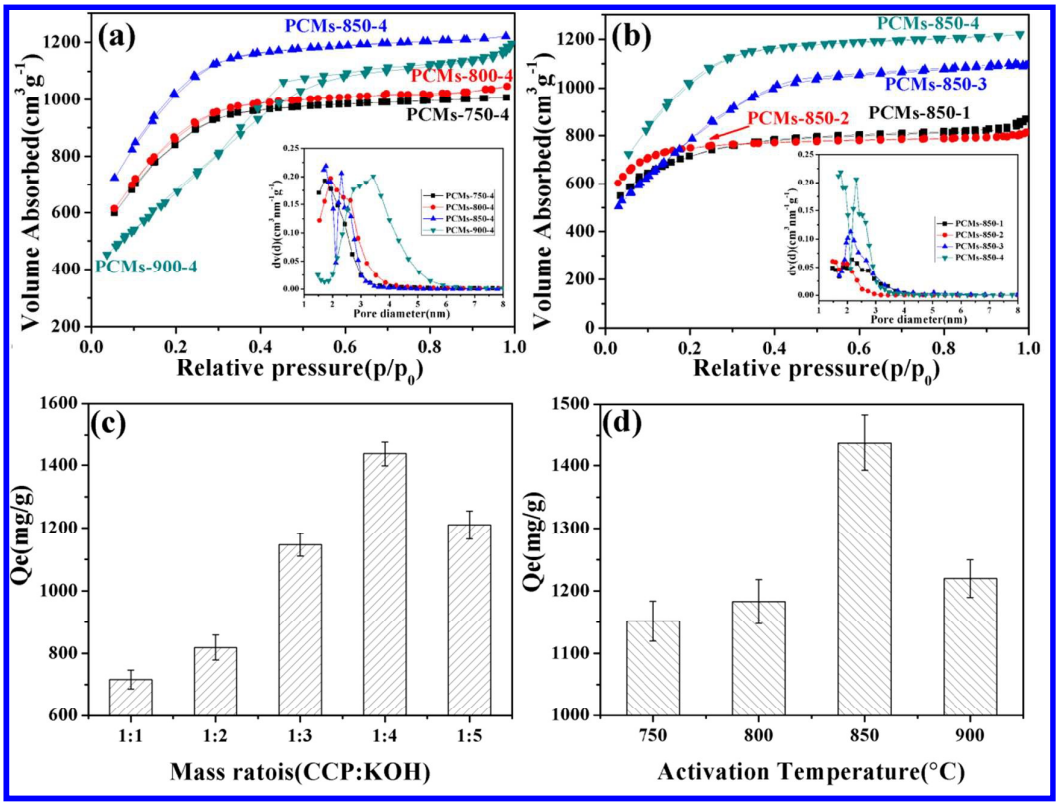

Fig. 2 (a，b) N_2 adsorption−desorption isotherms and pore size distributions (the DFT method) of PCMs-T-x, (c) Equilibrium absorption capacity of PCMs-850-x for TC, (d) Equilibrium absorption capacity of PCMs-T-4 for TC.

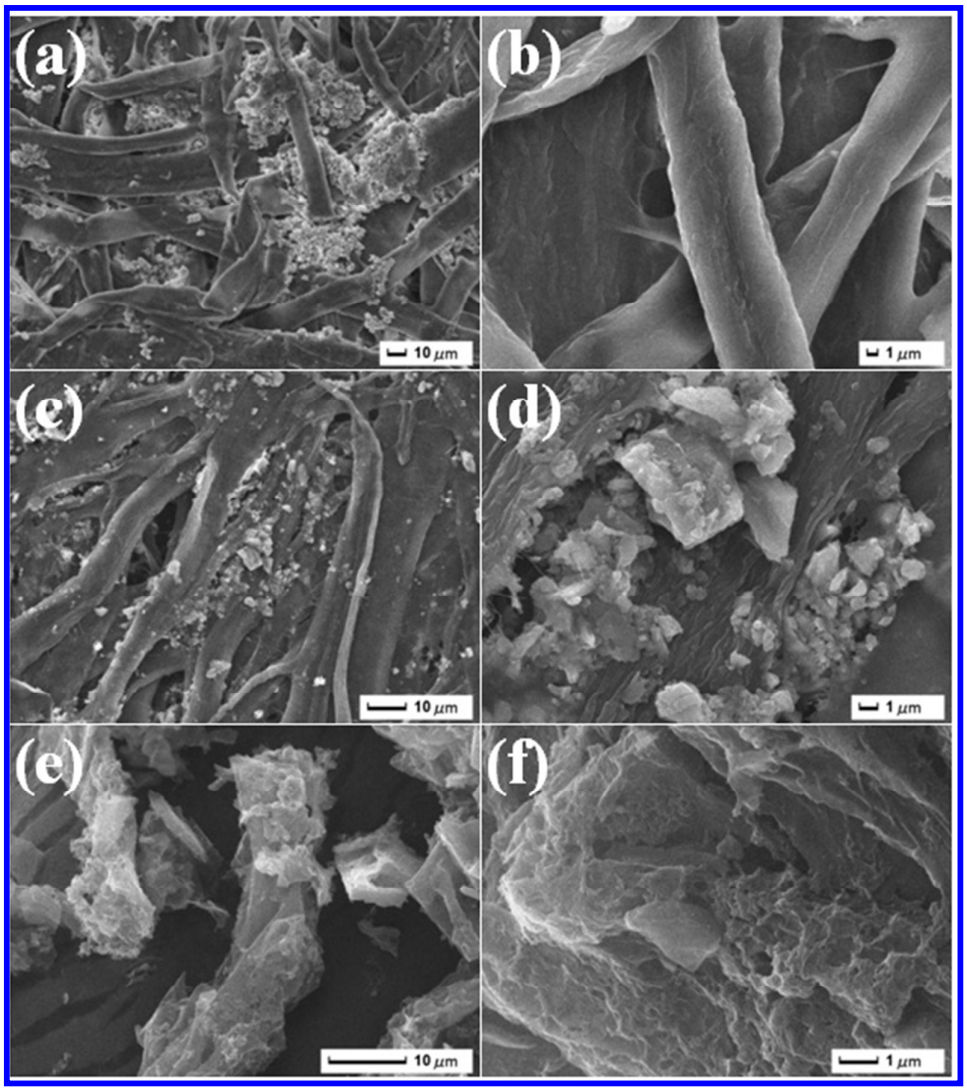

Fig. 3 SEM images of CP (a, b), CCP (c, d) and PCMs-850-4 (e, f).

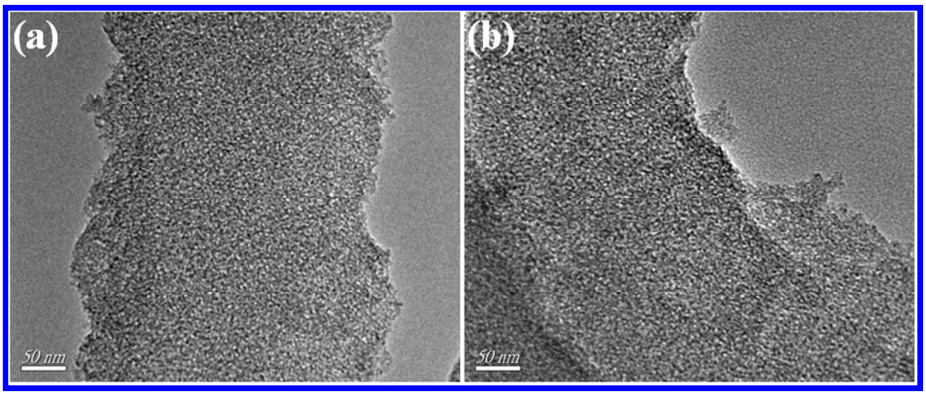

Fig. 4 TEM images of PCMs-850-4.

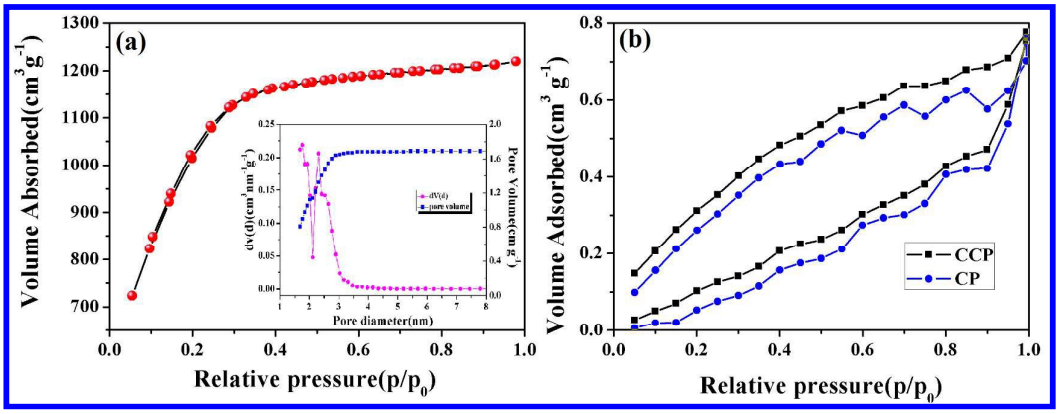

Fig. 5 N_2 adsorption−desorption isotherms of (a) PCMs-850-4, (b) CP and CCP.

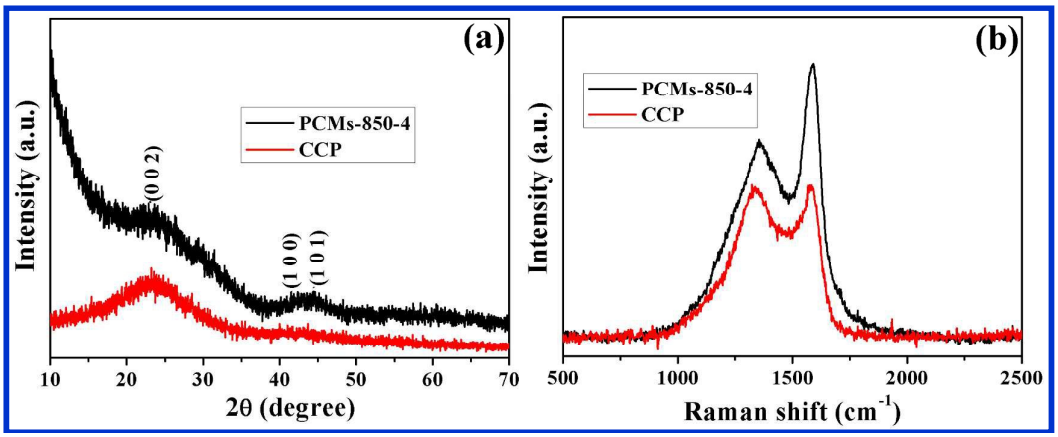

Fig. 6 XRD patterns (a) and Raman spectra (b) of CCP and PCMs-850-4.

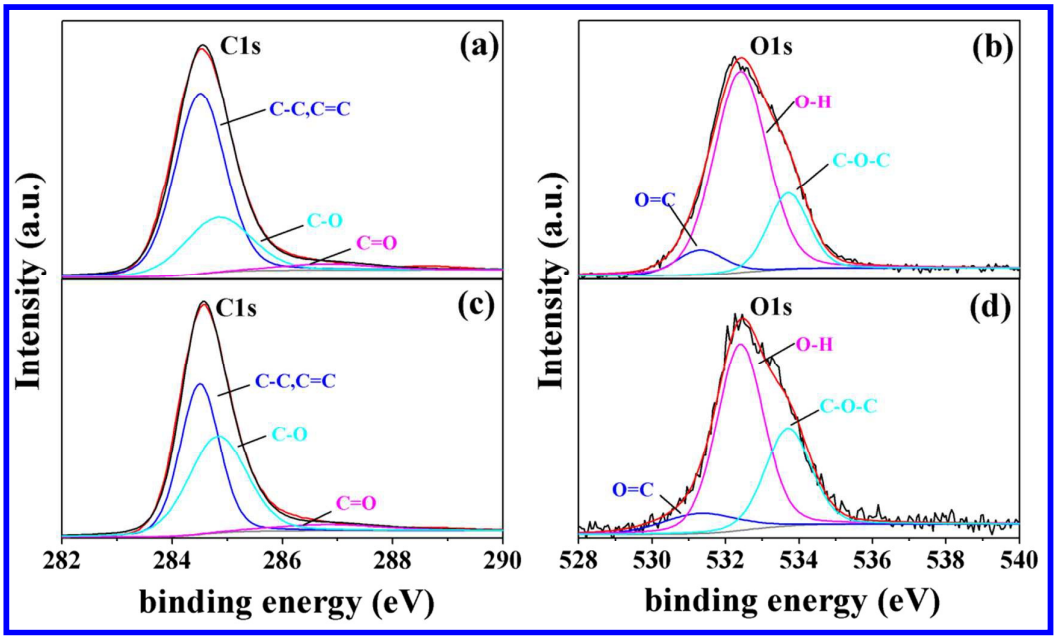

Fig. 7 High-resolution XPS spectra of CCP and PCMs-850-4.

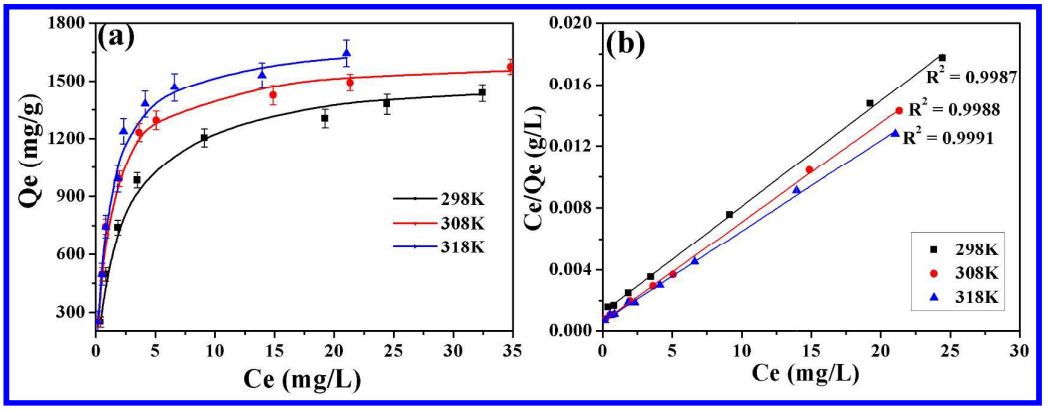

Fig. 8 (a) The non-linear fitting and (b) linear fitting curves of TC adsorption onto the PCMs-850-4 by Langmuir model at three different temperatures.

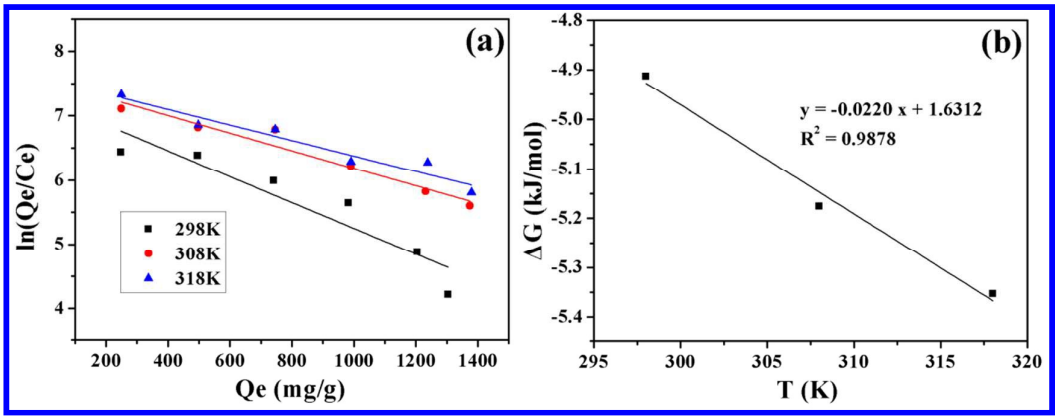

Fig. 9 (a) Fitting ln (Q_e/C_e) vs Q_e and (b) ΔG^{θ} was plotted against T.

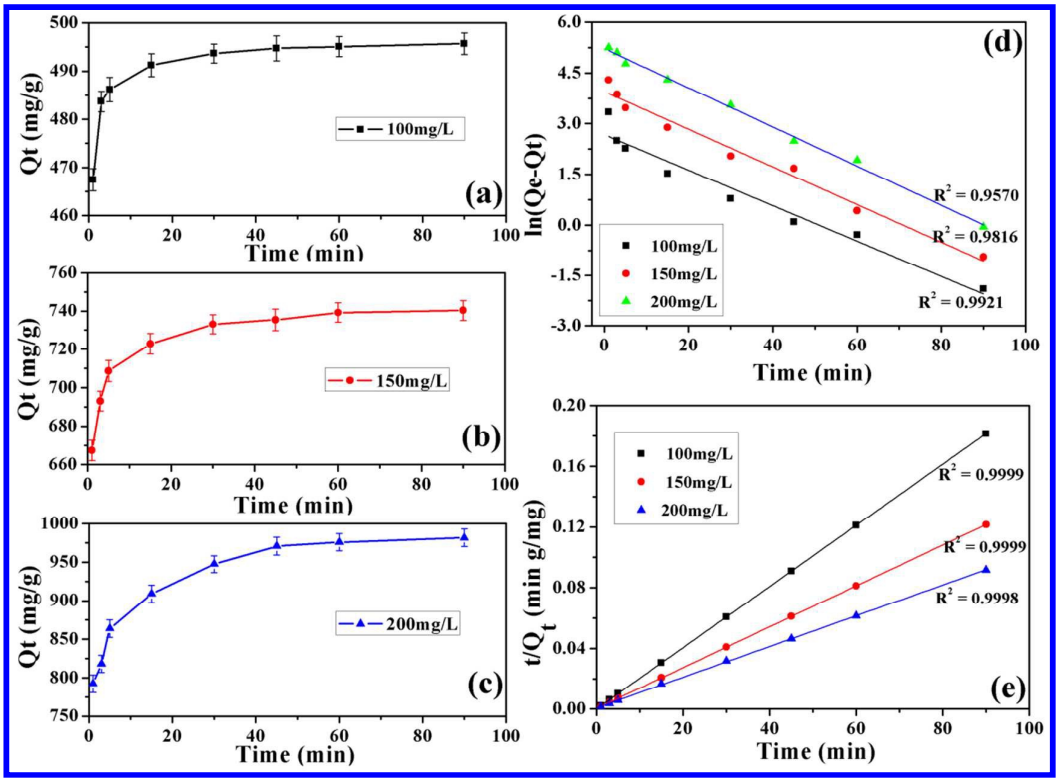

Fig. 10 The adsorption kinetics (a, b, c) and the linear-fitting kinetics curves for TC adsorption onto PCMs-850-4 by the pseudo-first-order (d) and pseudo-second-order (e) rate model with the different initial TC concentrations (C_0=100,150 and 200 mg/g) at 298 K.

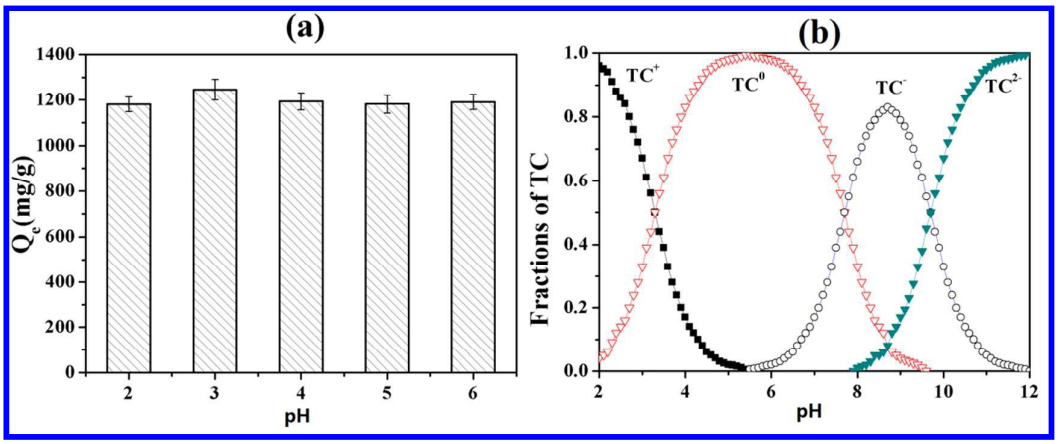

Fig. 11 (a) Influence of pH on TC adsorption onto PCMs-850-4, (b) Fractions of TC at different pH values.

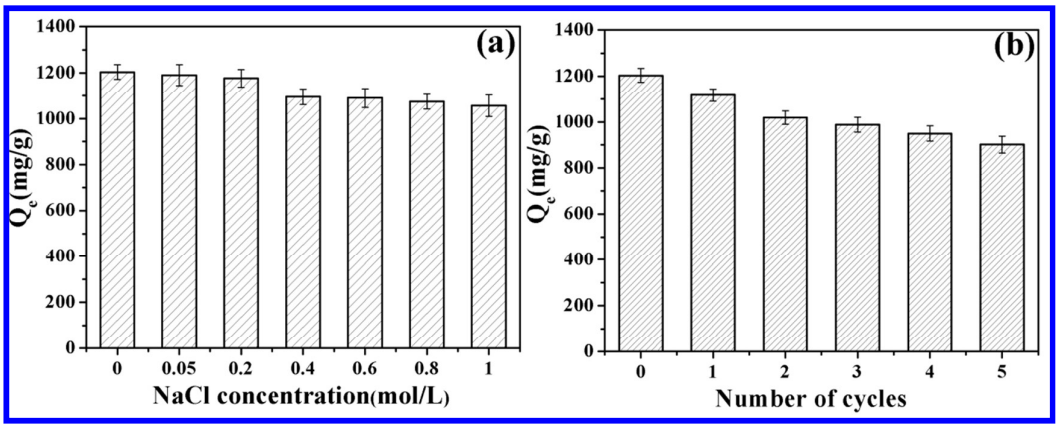

Fig. 12 (a) Effect of ionic strength on TC adsorption onto PCMs-850-4, (b) Reusability of PCMs-850-4.

Table 1 The porosity characteristics of PCMs-T-x synthesized at different parameters

Parameters	Specific surface area (m^2/g)	Micropore surface area (m^2/g)	Total pore volume (cm^3/g)	Micropore volume (cm^3/g)	Microporosity (%)	Average pore size (nm)
PCMs-750-4	2978.44	2,661.32	1.259	1. 390	89.35	1.645
PCMs-800-4	3,053.65	2,752.88	1.321	1. 442	90.15	1.982
PCMs-850-1	2,606.63	2,187.60	1.232	0.966	83.94	1.718
PCMs-850-2	2,866.05	2,695.57	1.281	1.096	92.79	1.867
PCMs-850-3	3,051.30	2,790.76	1.612	1.499	91.46	1.916
PCMs-850-4	3598.95	3302.89	1.887	1.632	91.77	2.002
PCMs-900-4	3,344.58	1,153.53	2.486	0.779	34.49	2.973

Table 2 Langmuir isotherm model parameters for TC

Langmuir isotherm model				
T (K)	$Q_{e,exp}$ (mg/g)	K_L (L/mg)	$Q_{e,cal}$ (mg/g)	R^2
298	1437.76	0.502	1497.01	0.9987
308	1575.88	0.843	1607.72	0.9990
318	1644.82	0.893	1709.4	0.9987

Table 3 Adsorption thermodynamics parameters for TC

T (K)	K_0	ΔG^0 (kJ/mol)	ΔH^0 (kJ/mol)	ΔS^0 (kJ/mol)
298	7.2635	-4.913		
308	7.5468	-5.175	1.631	0.022
318	7.5733	-5.353		

Table 4 Adsorption kinetics parameters for TC

C_0 (mg/L)	$Q_{e,exp}$ (mg g^{-1})	pseudo-first-order model			pseudo-second-order model		
		$Q_{e,cal}$ (mg g^{-1})	$K_1\times10^{-3}$ $(min)^{-1}$	R^2	$Q_{e,cal}$ (mg g^{-1})	$K_2\times10^{-5}$ (g mg^{-1} min^{-1})	R^2
100	495.83	14.49	52.5	0.9570	496.03	2.229	0.9999
150	740.73	51.89	55.7	0.9816	741.84	9.296	0.9999
200	982.65	181.16	56.7	0.9921	988.14	62.61	0.9999

Table 5 Adsorption capacity for TC of PCMs-850-4 compare with other adsorbents

Adsorbents	Q_m(mg/g)	Refs.
NaOH-activated carbon	455.33 (298K)	25
Clay	800 (298K)	44
Smectite	462 (298K)	45
C2	672.0 (298K)	46
ITAC-Fe	769.23 (298K)	47
GO	313 (298K)	48
PCMs-850-4	1437.76 (298K) 1575.88 (308K) 1644.82 (318K)	Present work

Graphical Abstract